Journal of Ovarian Research

RESEARCH

Open Access

Long-term 3D culture of human cumulus granulosa cell spheroids in PEGylated fibrin: a preclinical model for reproduction and ovarian research

Maria João Sousa[1], Katia Woinska[1], Thalles Fernando Rocha Ruiz[1,2], Maria Costanza Chiti[3], Arezoo Dadashzadeh[1], Hanne Vlieghe[1], Christine Wyns[1,3], Hugo Vankelecom[4] and Christiani A. Amorim[1*]

Abstract

Background Cumulus granulosa cells (CGCs) are essential for oocyte support, metabolic cooperation, and steroidogenesis, yet they deteriorate rapidly in conventional 2D culture, limiting long-term studies of these human ovarian somatic cells. Existing 3D systems rarely focus specifically on CGCs or sustain their function over extended periods. Here we developed a novel hCGC spheroid model encapsulated in PEGylated fibrin hydrogel, a stable, ovarian tissue-like biomaterial, to sustain viability, architecture, and endocrine activity over 30 days, providing a preclinical somatic platform for ovarian biology, reproductive toxicology, and fertility-preservation strategies.

Results By day 6, hCGCs self-assembled into compact spheroids expressing granulosa markers AMHR2 (96.98 ± 4.57% positive cells) and CYP19A1 (75.43 ± 7.85% positive cells) and depositing extracellular matrix components (collagen III, collagen IV, fibronectin, and hyaluronan; HA area fraction 31.25 ± 8.06%). After encapsulation in PEGylated fibrin, spheroids maintained spherical geometry and structural integrity for 30 days. Spheroid area and solidity increased significantly by day 15 before stabilizing, while roundness remained high. Metabolic activity stayed stable across 30 days, and day-30 viability was 89.4 ± 4.4%, with only 10.6 ± 4.4% dead area. Estradiol secretion increased from 250 ± 38 pg/mL (day 3) to a peak of 370 ± 45 pg/mL (day 12), then progressively declined to 120 ± 25 pg/mL by day 30, with a significant time-dependent effect.

Conclusion This study presents the first long-term 30-day 3D culture system designed for human CGCs in an oocyte-independent context, preserving high viability, compact architecture, intercellular communication, and dynamic steroidogenic function. The model offers a robust, oocyte-independent preclinical tool for investigating CGC-specific mechanisms, screening reproductive toxicants, and optimizing somatic support in fertility-preservation approaches such as ovarian tissue-based in vitro maturation.

Keywords Cumulus granulosa cells, 3D spheroid culture, PEGylated fibrin hydrogel, Steroidogenesis, Extracellular matrix, Tissue engineering, Fertility preservation

*Correspondence:
Christiani A. Amorim
christiani.amorim@uclouvain.be

Full list of author information is available at the end of the article

Introduction

The ovarian follicle, the ovary's functional unit, is composed of an oocyte surrounded by somatic cells. In the primordial and primary stages, these somatic cells consist solely of granulosa cells, while in secondary and later stages, a theca cell layer develops, and together these cells provide essential endocrine and paracrine support [1, 2]. Within the granulosa population, two subtypes can be distinguished: mural granulosa cells (MGCs), which line the follicular wall, and cumulus granulosa cells (CGCs), which directly envelop the oocyte to form the cumulus-oocyte complex (COC) [1, 3]. Through gap junctions and transzonal projections, CGCs regulate oocyte nutrient transfer, meiotic progression, and cytoplasmic maturation [4, 5], while also secreting extracellular matrix (ECM) components, such as hyaluronan (HA), essential for cumulus expansion and fertilization [6]. Although MGCs are classically associated with steroidogenesis, CGCs are not merely supportive cells, they also retain to steroidogenic capacity, particularly in the peri-ovulatory period [7]. The health and function of CGCs are therefore pivotal for oocyte competence, embryo development, and fertility.

The COC is indispensable in reproductive physiology and assisted reproductive technologies (ART) [8]. Studying CGCs in vitro could provide valuable insights into somatic cell signaling, metabolic cooperation, steroidogenesis, and the influence of environmental or pharmacological exposures. Robust CGC culture systems represent a valuable target for developing preclinical models. These models facilitate applications in reproductive biology and fertility preservation, where understanding somatic support mechanisms may help redefine approaches such as in vitro maturation (IVM), in specific clinical contexts, including polycystic ovary syndrome (PCOS), or research related to ovarian tissue oocyte-IVM (OTO-IVM) during ovarian tissue cryopreservation (OTC), where the behavior of somatic cells may influence the maturation potential of oocytes recovered from tissue [9, 10]. Studies using co-culture have shown that the presence of CGCs can influence the environment surrounding immature oocytes [11–13], underscoring the importance of understanding CGC physiology itself. However, human CGC-specific culture systems remain limited, and their independent biology is still poorly characterized. Progress in this field has been constrained by the restricted availability of CGCs from ART cycles, their low proliferative capacity, and their fast degeneration in conventional 2D systems. Early studies reported human CGCs (hCGCs) survival for a few days in 2D [14], and although more recent work has extended culture to 30 days, these models demonstrated increasing activation of apoptotic and ageing pathways over time [15]. These limitations underscore the need for stable, physiologically relevant 3D CGC models capable of supporting long-term viability, organization, and endocrine function, providing platforms for preclinical research, drug and toxicology screening, and mechanistic studies of granulosa cell (GC) biology.

Three-dimensional (3D) culture systems offer an attractive alternative, as they provide a more physiological microenvironment that promotes cell-cell interactions, supports ECM deposition, and better preserves cellular functions compared with 2D monolayers [16–18]. Recent advances in ovarian 3D models have underscored the potential of such platforms for modeling folliculogenesis, endocrine disruption, and fertility preservation, yet dedicated long-term models for isolated hCGCs, free from oocyte or MGC influences, remain scarce. Spheroid models are particularly attractive for ovarian research, as GCs can self-aggregate mimicking the 3D arrangement of the physiological COCs. In ovarian biology, 3D systems using MGCs or even whole follicles showed improved survival and hormone secretion when compared with 2D [18]. For example, MGC spheroids in bovine models sustained steroidogenesis [19], and in felids, they supported luteinization with estradiol and progesterone production for several days [20]. Human 3D models, often using MGCs or immortalized granulosa tumor lines, such as KGN cells, achieved limited estradiol production [21, 22]. Critically, long-term 3D systems dedicated specifically to hCGCs are scarce, leaving gaps in tools for studying CGCs behavior outside the oocyte context.

To overcome these limitations, biomaterials like hydrogels have been explored for providing a hydrated, ovarian-tissue–like environment that supports the culture of ovarian somatic cells. Fibrin, with its integrin-binding motifs [23], is an interesting candidate, but degrades rapidly. PEGylated fibrin overcomes this limitation though covalent modification of the fibrinogen with polyethylene glycol (PEG), which shows slower enzymatic degradation, increases mechanical stability, and allows tuning of matrix elasticity while preserving bioactivity [24–26]. Recent studies demonstrated that pegylated fibrin hydrogel provided higher stability and ovarian tissue-like mechanics, successfully sustaining stromal cells and follicles in extended culture [26, 27].

To address these critical gaps, this study aimed to develop a 3D hCGC spheroid platform encapsulated in PEGylated fibrin hydrogel. The objective was to establish a durable somatic preclinical system capable of maintaining CGC viability, structural organization, and steroidogenic activity over an extended culture period. This proof-of-concept model provides a foundation for future investigations into hCGC biology, endocrine regulation, reproductive toxicology, and the somatic factors that contribute to follicular physiology in controlled experimental environments.

Materials and methods

Ethical statement

The use of human cumulus granulosa cells (hCGCs) was approved by the Institutional Review Board (IRB) of the Université Catholique de Louvain on 3 June 2019 (IRB reference 2014/16DEC/597). As these cells constitute anonymised residual human material obtained during routine IVF/ICSI procedures and would otherwise be discarded, the need for informed consent was waived by the IRB in accordance with applicable Belgian regulations.

Patient material

COCs were obtained during routine oocyte retrieval procedures at the IVF Department of the Cliniques universitaires Saint-Luc (Brussels, Belgium). Patients were 22–42 years old. Controlled ovarian stimulation was performed using a gonadotropin-releasing hormone (GnRH) antagonist protocol, with gonadotrophins administrated in the late follicular phase. Final oocyte maturation was triggered with human chorionic gonadotropin (hCG) until at least one follicle reached a mean diameter of 15 mm. Serum estradiol levels on the day of trigger had a median of 1198 pg/ml (IQR 874–1554 pg/ml). For clinical purposes, cumulus cells were enzymatically removed from oocytes using HYASE-10 × (26284, Vitrolife, Londerzeel, Belgium), diluted 1:10 in prewarmed Sperm Preparation Medium (10700060, Origio, Måløv, Denmark), and then mechanically dissociated sequentially using 600 µm, 170 µm, and 130 µm Flexipettes (Cook Medical, Limerick, Ireland) to ensure complete removal of cumulus cells. The isolated cells were washed twice in pre-warmed Sperm Preparation Medium to eliminate residual enzyme. Oocytes were immediately returned to the embryologists for vitrification or ART procedures, while the CGCs were collected and transported to the research laboratory for further culture (see workflow in Fig. 1).

Moreover, human placenta and umbilical cord formalin-fixed, paraffin-embedded sections were kindly provided by a colleague from the Cliniques universitaires Saint-Luc (UCLouvain), with appropriate ethical approval and informed consent. The tissue served as a physiological reference control for immunofluorescence analyses.

Spheroid formation

CGCs were pooled from 4 to 6 patients to generate one production (hereafter referred to as one biological replicate). Cells from each production were processed independently, washed and resuspended in spheroid culture medium [DMEM/F12 (21041-025, Gibco, Paisley, UK) supplemented with 5% KnockOut™ Serum Replacement (KSR; 10828-010, Gibco), 1% Antibiotic-Antimycotic (15240-062, Gibco), 1% Insulin-Transferrin-Selenium (ITS; 41400-045, Gibco), 2% L-Glutamine (25030-024, Gibco), 100 ng/mL IGF-1 (100 – 11, PeproTech, New Jersey, USA) and 5 IU/mL of Menopur (Ferring, Aalst, Belgium)]. Cells were seeded at a density of 2000 cells per

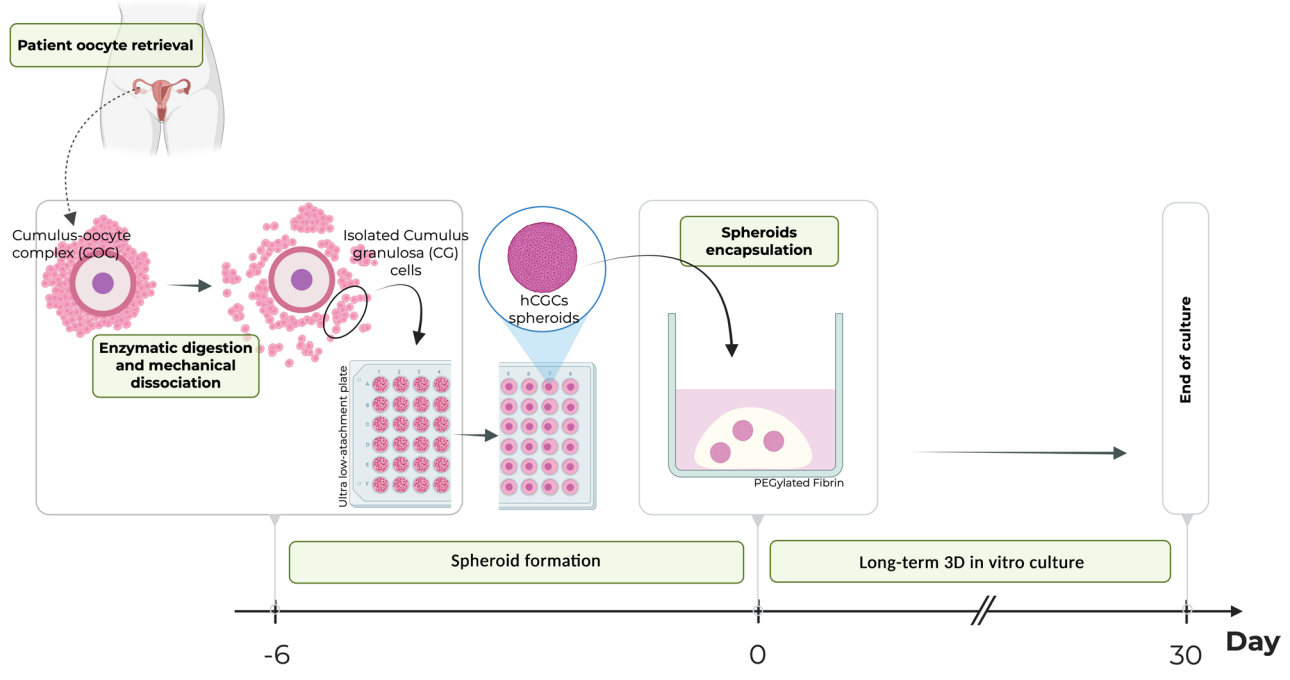

Fig. 1 Experimental workflow for hCGC spheroid culture. Schematic representation of the experimental process: COCs were obtained from IVF/ICSI patients at Saint-Luc University Hospital and treated with hyaluronidase to isolate CGCs. Isolated CGCs were seeded in ultra-low attachment plates to form spheroids over 6 days, followed by encapsulation in PEGylated fibrin hydrogel for long-term 3D culture (up to 30 days). Created with BioRender.com

well in 96-well ultra-low attachment plates (83.3925.400, Sarstedt, Nümbrecht, Germany) and cultured for 6 days at 37 °C in a humidified atmosphere of 5% CO_2. Half of the medium was refreshed every other day. At day 6, a subset of spheroids was allocated to immunofluorescence analysis, while the remaining spheroids were encapsulated in PEGylated fibrin for long-term culture.

Spheroid characterization

Histological procedure and immunofluorescence

The hCGC spheroids were fixed in 4% paraformaldehyde (PFA) for 1 h at room temperature (RT), processed, and embedded in paraffin. Blocks were sectioned at 5 µm and mounted on adhesion slides to further immunofluorescence analysis and Alcian blue staining. After deparaffinization, autofluorescence was quenched with 50 mM NH_4Cl. Antigen retrieval was performed using either citrate or Tris-EDTA buffer as appropriate for each antibody. All antibody-specifications are detailed in Table 1. Sections were permeabilized, blocked, and incubated overnight at 4 °C with the primary antibodies. After washing, fluorophore-conjugated secondary antibodies were applied for 45 min at RT. Slides were mounted using Fluorshield™ with DAPI (F6057, Sigma-Aldrich, St. Louis, MO, USA). Human placental villi served as positive controls for ECM staining, and ovarian tissue containing follicles served as positive controls for AMHR2 and aromatase. Negative controls were processed in parallel with the primary antibodies omitted. Images were captured using a fluorescent microscope and analyzed using ImageJ software (v1. 54q).

Table 1 Antibody specifications for immunofluorescence analysis

Antibody ID	Supplier, Cat#	Working Dilution	Antigen retravel
AMHR2 Polyclonal Antibody	ThermoFisher, PA5-119934	1/100	Tris-EDTA (pH 9)
CYP19 Antibody (E-9)	Santa Cruz, sc-374,176	1/75	Tris-EDTA (pH 9)
Anti-Connexin 43 Antibody	Merck, C6219	1/250	Citrate Buffer (pH 6)
Anti-Collagen IV antibody	Abcam, ab6586	1/150	Citrate Buffer (pH 6)
Anti-Laminin antibody	Abcam, ab11575	1/200	Tris-EDTA (pH 9)
COL3A1 (E8D7R) XP® Rabbit mAb (Alexa Fluor® 555 Conjugate)	Cell Signaling, #76,735	1/100	Citrate Buffer (pH 6)
Anti-Fibronectin antibody	Abcam, ab23750	1/100	Tris-EDTA (pH 9)
Goat anti-Rabbit IgG (H + L) Highly Cross-Adsorbed Secondary Antibody, Alexa Fluor™ 488	ThermoFisher, A-11,034	1/250	
Goat anti-Mouse IgG (H + L) Highly Cross-Adsorbed Secondary Antibody, Alexa Fluor™ 594	ThermoFisher, A-11,032	1/250	
Goat anti-Rabbit IgG (H + L) Cross-Adsorbed Secondary Antibody, Alexa Fluor™ 594	ThermoFisher, A-11,012	1/250	

Alcian blue staining with hyaluronidase treatment

Paraffin sections of hCGC spheroids and human umbilical cord tissue were deparaffinized and rehydrated. For the enzymatic control, paired sections were incubated with bovine testicular hyaluronidase (~ 500IU/mL, pH 5.5; H3506, Sigma-Aldrich) for 60 min at 37 °C. All sections were stained with 1% Alcian Blue 8GX (4500094527, Thermo Fisher, Kandel, Germany) in 3% acetic acid (pH 2.5; 695092, Sigma-Aldrich) for 40 min at RT. Counterstaining was performed with Nuclear Fast Red (60700, Sigma-Aldrich) for 5 min. Samples were dehydrated, cleared, and mounted. Images were captured using a 3DHistech SCAN II microscope and analyzed with ImageJ software. For each spheroid, a region of interested (ROI) was drawn, and the Alcian blue channel was isolated by color deconvolution. Mean intensity was measured on paired sections processed without and with hyaluronidase treatment. The HA-sensitive fraction was expressed as a percentage:

$$HA\% = 100 \times \frac{AB_{-HYALU} - AB_{+HYALU}}{AB_{-HYALU}}$$

Synthesis of PEGylated fibrinogen and hCGC spheroid's encapsulation

PEGylated fibrinogen was synthesized following our previously reported protocol [27]. In brief, human fibrinogen (F3879, Sigma-Aldrich) was dissolved in PBS (10010-015, Gibco) at 85 mg/mL and incubated for 2 h at 37 °C. The solution was then sterilized by passage through a 0.20-µm syringe filter. In parallel, a solution of O, O′-Bis[2-(N-succinimidyl-succinylamino) ethyl] polyethylene glycol (NHS-PEG-NHS, 2,000 Da; 713783, Sigma-Aldrich) was prepared in PBS at 5 mg/mL and similarly filtered. Equal volumes of fibrinogen and NHS-PEG-NHS solutions were combined, yielding a 10:1 molar ratio, mixed gently, and incubated at 37 °C for 2 h to allow PEGylation. Then, 3 spheroids were added to PEGylated fibrinogen solution, resulting in a final fibrinogen concentration of about 39.13 mg/mL. Gelation was induced by adding the same volume of thrombin (50.36 IU/mL), prepared by reconstitution and dilution of human thrombin (T7009, Sigma-Aldrich) in 40 mM $CaCl_2$. The mixtures were incubated at 37 °C for 15 min to complete polymerization prior to adding the culture medium. Spheroids were maintained

in culture for 30 days at 37 °C in a humidified atmosphere of 5% CO_2, using the same spheroid culture medium, which was replaced every third day. (Fig. 1).

Morphological analysis

Images of cultured hCGC spheroids were taken at days 0, 15 and 30 using an inverted microscope (Leica DMIL, Diegem, Belgium) and analyzed by ImageJ software after spatial calibration. Individual spheroids were manually segmented using the freehand selection tool to generate single-spheroid regions of interest (ROIs). Images were converted to 8-bit grayscale, and intensity thresholding was applied to generate binary masks. Morphological parameters, including area, roundness, and solidity, were quantified using the *Analyze Particles* function.

Cell viability and metabolic activity

After 30 days of hCGCs spheroid culture in PEGylated fibrin, the hydrogels were washed to remove any surround media and incubated with a Live/Dead™ solution (5 µM ethidium homodimer-1 and 2 µM calcein-AM in PBS; Molecular Probes, Leiden, The Netherlands) for 45 min at 37 °C in 5% CO_2. Spheroids were imaged on an inverted microscope (Leica DMIL), and images were analyzed in ZenBlue v3.10 and ImageJ software. For each spheroid, an ROI was drawn. Mean fluorescence was recorded in the calcein and EthD-1 channels, and viability was estimated from the relative green versus red area within the ROI.

For metabolic activity analysis, measurements were performed every third day prior medium change. The culture medium was replaced with PrestoBlueTH (P50200, Thermo Fisher) diluted in spheroid medium at 1:10 ratio. After 2 h incubation at 37 °C, metabolic rate was quantified by fluorescent spectroscopy at excitation and emission wavelengths of 560 nm and 620 nm, respectively. Normalization was performed using a PEGylated fibrin drop without spheroids but cultured in the same conditions.

Hormone secretion analysis

During long-term culture of the hCGC spheroids, medium was collected on days 3, 12, 21 and 30 after encapsulation, immediately before medium change, and stored at -80 °C until analysis. 17β-estradiol was quantified using ELISA (ADI-900-008, Enzo, New York, NY, USA) following the manufacturer's instructions. Standard and samples were run in duplicate.

Statistical analysis

Quantitative data are presented as mean ± SEM, unless otherwise stated. Statistical analyses were performed using GraphPad Prism version 10.0 (GraphPad Software, USA). For each dataset, normality of distribution was first evaluated using the Shapiro-Wilk test. When data were normally distributed and sample size was sufficient, parametric tests (one-way ANOVA) were applied, followed by Tukey's post hoc test for pairwise comparisons. When assumptions of sphericity were not met in repeated measures, the Geisser-Greenhouse correction was applied. For datasets with small sample size or non-normal distribution, Friedman's test with Dunn's multiple comparisons was used. No formal power calculations were conducted due to the exploratory nature of the study and limited cell availability. A p-value < 0.05 was considered statistically significant.

Results

hCGC spheroids display compact morphology and retain granulosa- specific markers

hCGCs were obtained from patients with mean age 34.5 ± 5.3 years (median 35, IQR 33-37.5). Spheroids, formed over 6 days in ultra-low attachment plates, exhibited compact, rounded morphology with defined borders (Fig. 2A). Immunofluorescence analyses at day 6, revealed strong expression of granulosa-specific markers Anti-Müllerian hormone receptor type 2 (AMHR2) and aromatase (CYP19A1), confirming steroidogenic potential (Fig. 2B). Day-6 immunofluorescence showed robust expression of granulosa markers AMHR2 and CYP19A1 across multicell layers within the spheroids, consistent with a preserved steroidogenic phenotype (Fig. 2B). Quantitatively, the proportion of marker-positive cells per spheroid was 96.98 ± 4.57% for AMHR2 and 75.43 ± 7.85% for CYP19A1, indicating near-ubiquitous AMHR2 and widespread CYP19A1 expression across the spheroid cell population.

ECM deposition and HA accumulation support spheroid compaction

Immunofluorescence at day 6 showed connexin-43 (Cx43) at cell-cell borders, indicating intercellular gap junctional communication. ECM components, including collagen III, fibronectin, and collagen IV, were detected throughout the spheroids, while laminin expression was negligible (Fig. 3A).

Alcian Blue staining confirmed HA accumulation in intercellular spaces (Fig. 3B). Quantitative analysis showed an HA-sensitive fraction of 31,25 ± 8,06% (Table 2), with variability (range: 18,70%-43,39%). These results indicate that hCGC spheroids actively deposit ECM, supporting early compaction by day 6.

Mean pixel intensity was measured in spheroid sections processed without ($AB\text{-}_{HYALU}$) or with hyaluronidase (AB_{+HYALU}). The HA fraction (HA%) represents the relative reduction in intensity post-digestion. Each line shows values for individual spheroid. Spheroids were obtained from 3 independent biological replicates ($n = 3$),

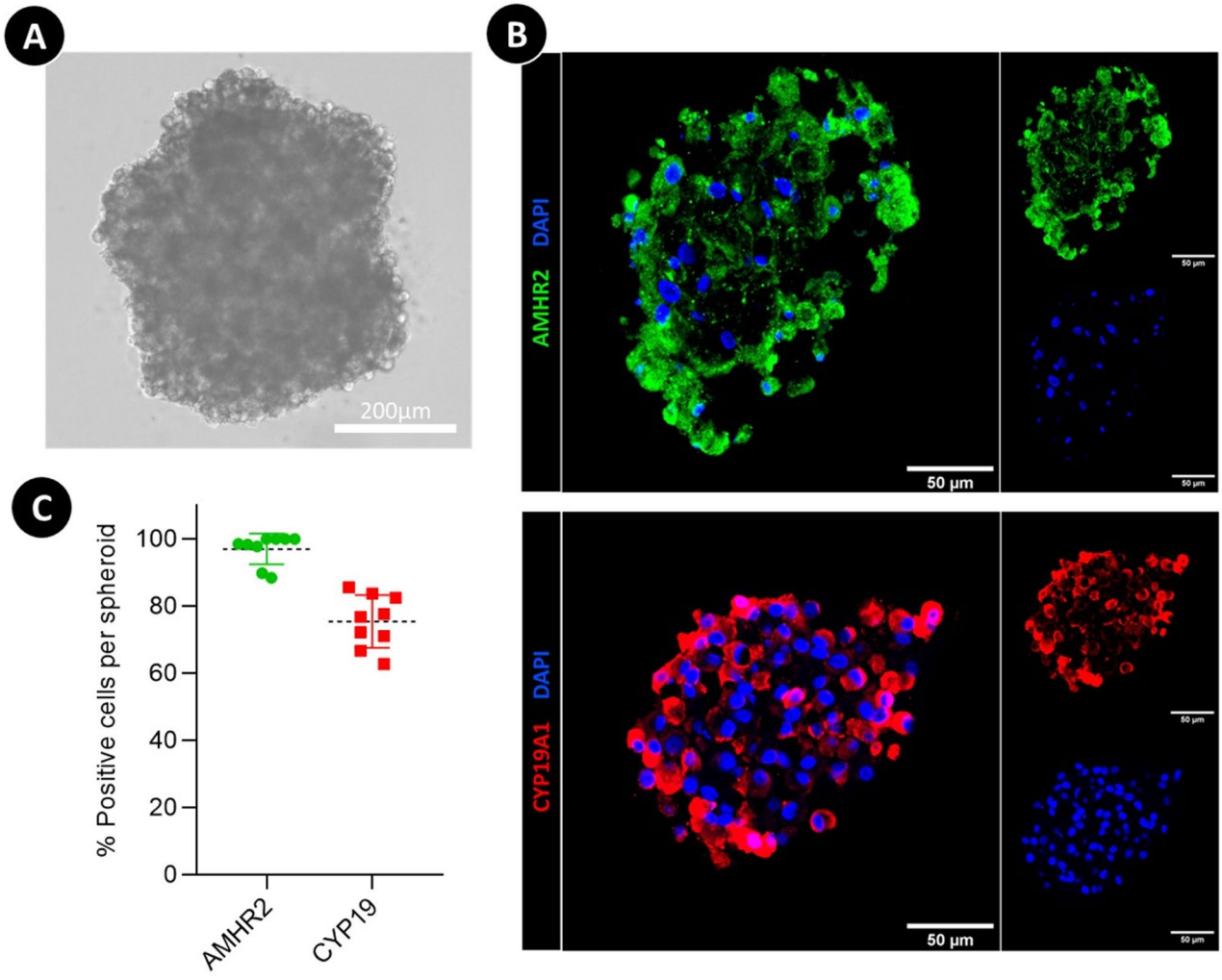

Fig. 2 Characterization of hCGCs cell spheroids. **A** Brightfield image of a day-6 hCGCs spheroid showing compact morphology. Scale bar: 200 µm. **B** Immunofluorescence staining for AMHR2 (green) and CYP19A1 (red), with nuclei counterstained with DAPI (blue). Scale bar: 50 µm. **C** Quantification of % positive cells per spheroid for AMHR2 (green) and CYP19 (red). Each dot represents an individual spheroid. Three independent biological replicates ($n = 3$) were analysed, each comprising three hCGCs spheroids from 4-6- patients. Measurements were averaged to yield a single value per replicate. Data are mean ± SEM

with 2–3 spheroids analyzed per replicate. Measurements within each construct were averaged to yield one value per biological replicate. Data are represented as mean ± SD.

Long-term culture in PEGylated fibrin maintains morphology and structural organization

Day-6 hCGC spheroids were encapsulated in PEGylated fibrin hydrogels, selected for their ovarian tissue-like mechanics and stability. Brightfield imaging revealed structural integrity over 30 days (Fig. 4A). Spheroids increased in area from day 0 to day 15 ($p < 0.01$), followed by a decrease by day 30 toward values closed to baseline (Fig. 4B). Roundness remained high, indicating consistent spherical geometry (Fig. 4C). Solidity increased significantly by day 15 ($p < 0.01$) and subsequently decrease by day 30, approaching baseline value of day 0 (Fig. 4D), reflecting sustained compaction.

hCGC spheroids remain viable and metabolically stable

Metabolic activity, assessed via PrestoBlue assay, remained stable over 30 days (relative absorbance 560–620 nm, normalized to PEGylated fibrin control, $p > 0.05$) (Fig. 5A). At day 30, Live/Dead staining showed strong calcein-AM fluorescence (viable cells) and minimal Ethidium homodimer-1 staining (dead cells) (Fig. 5B). Quantitative analysis confirmed high viability (89.4 ± 4.4% viable area vs. 10.6 ± 4.4% dead area) (Fig. 5C).

Pegylated-fibrin supports long-term estradiol secretion

17β-estradiol secretion was quantified via ELISA at days 3, 12, 21, and 30 (Fig. 6). In 3D cultures, estradiol levels

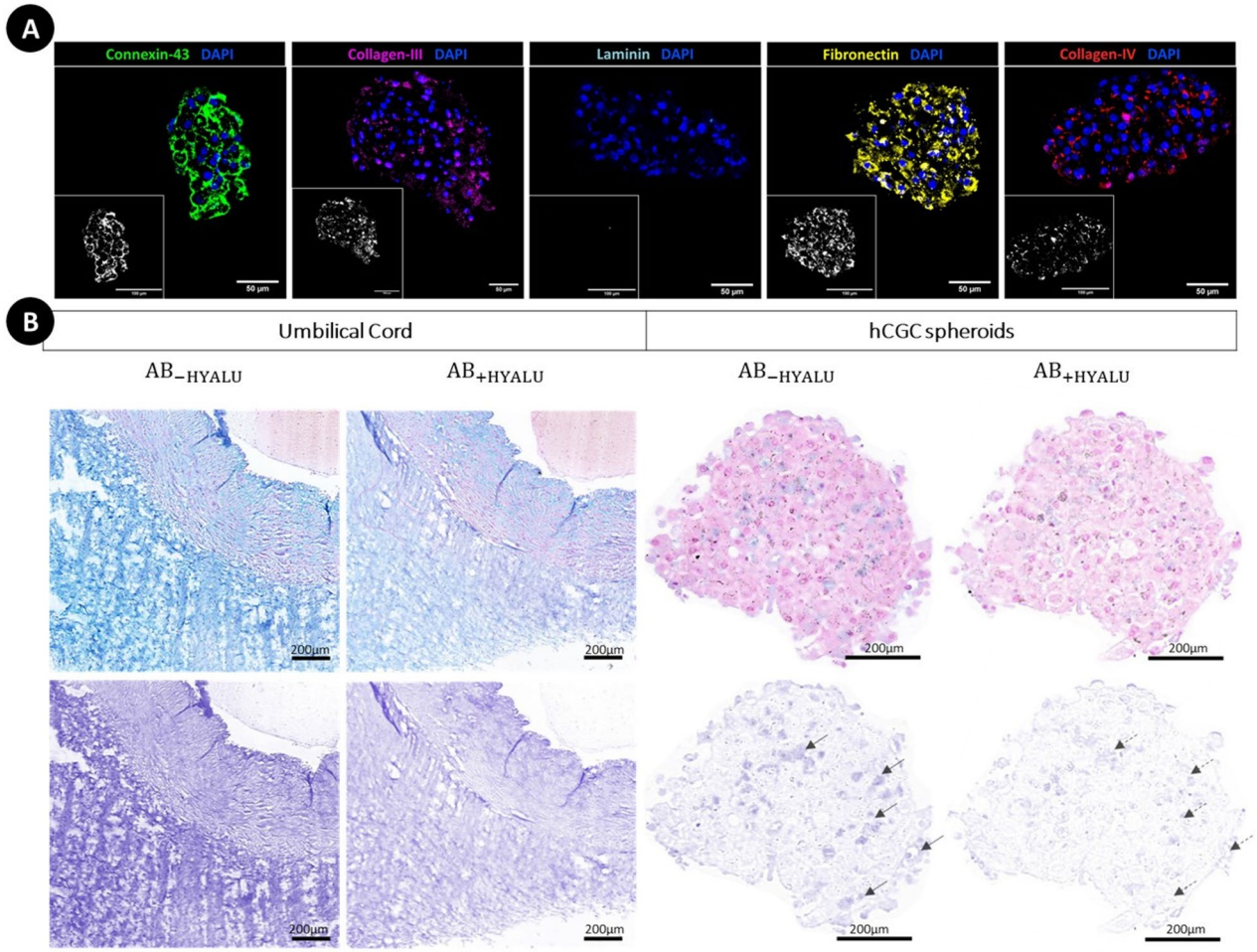

Fig. 3 Early ECM deposition in hCGC spheroids. **A** Immunofluorescence staining at day 6 showing Cx43 (green), collagen-III (pink), collagen-IV (red), fibronectin (yellow), and laminin (cyan, negligible). Nuclei were counterstained with DAPI (blue). Scale bars: 100 µm. Inserts show single-color channels. **B** Alcian Blue staining of hCGCs spheroids (right) and human umbilical cord control (left), with Nuclear Fast Red counterstain. Sections were processed without (AB_{-HYALU}) or with hyaluronidase (AB_{+HYALU}) to confirm HA specificity. Scale bars: 200 µm. In both umbilical cord and spheroid samples, staining was assessed in paired conditions (with vs. without hyaluronidase) to distinguish HA-dependent signal from background staining

Table 2 Quantification of Alcian Blue staining intensity in hCGC spheroids

Alcian Blue mean intensity without treatment (AB_{-HYALU})	Alcian Blue mean intensity with hyaluronidase treatment (AB_{+HYALU})	HA%
11.957	7.48	37.44%
29.356	16.619	43.39%
40.546	30.369	25.10%
21.095	14.036	33.46%
19.951	13.696	31.35%
36.855	26.05	29.32%
26.588	21.616	18.70%
	Mean	31.25 ± 8.06%

peaked at 370 ± 45 pg/mL (day 12) from 250 ± 38 pg/mL (day 3), declining to 320 ± 40 pg/mL (day 21) and 120 ± 25 pg/mL (day 30) ($p = 0.0174$, Friedman's test, Kendall's W = 0.30). Although no significant pairwise differences were detected (Dunn's test, $p > 0.0685$), which is expected when working with only three biological replicates, the overall Friedman's test still demonstrates a significant time-dependent change in 17β-estradiol secretion.

Discussion

This study establishes a pioneering 3D hCGC spheroid model in PEGylated fibrin hydrogel, sustaining high viability, compact morphology, expression of granulosa markers AMHR2 and CYP19A1, and dynamic estradiol secretion over 30 days. The model recapitulates key aspects of the COC microenvironment, including Cx43-mediated gap junctions for intercellular communication and ECM deposition (collagen III/IV, fibronectin, HA) supports spheroid compaction and function.

Compared to 2D cultures, where hCGCs degenerate within days [14], this 3D system markedly extends

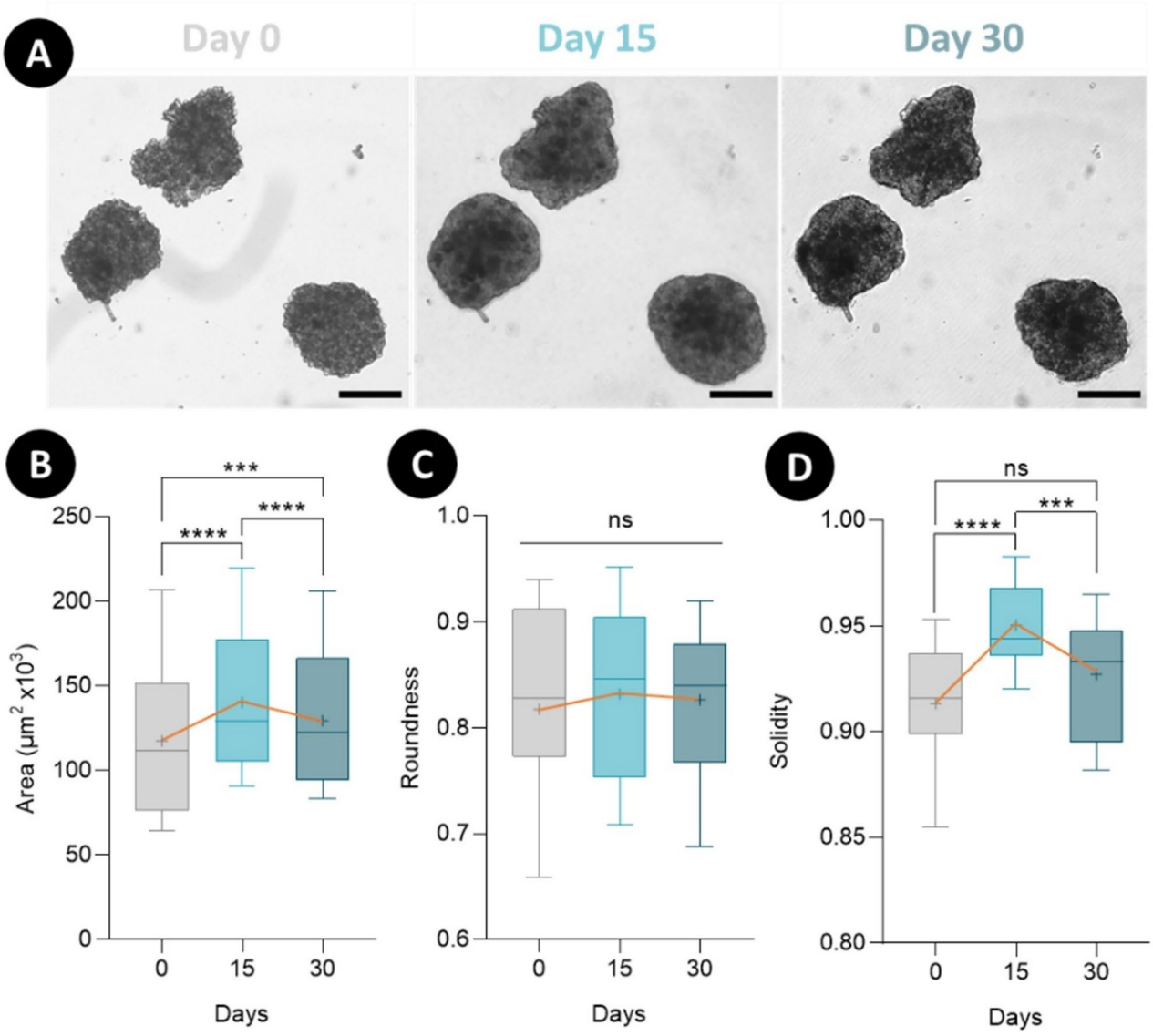

Fig. 4 Morphological changes in hCGCs spheroids over time. **A** Brightfield images at days 0, 15, and 30. Scale bar = 200 µm. **B**-**D** Box-and-whisker plots showing area, roundness, and solidity ($n = 5$ biological replicates; each biological replicate consisted of one PEGylated fibrin construct containing 3 hCGC spheroids from a pool of 4–6 patients). Measurements within each construct were averaged to yield one value per biological replicate. Median (line), interquartile range (box), min/max (whiskers), and mean (+) are shown. Orange lines indicate mean trends. Statistical analysis: one-way ANOVA with Tukey's multiple comparisons test. *$p < 0.05$, **$p < 0.01$, ***$p < 0.001$, ****$p < 0.0001$; ns = not significant

viability and functionality. Tahajjodi et al. [28] reported AMHR2 and CYP19A1 expression in freshly isolated hCGCs, with short-term 2D culture (48 h) increasing AMH secretion. In our model, these markers were maintained at day 6, suggesting preservation of key granulosa cell characteristics. Strong Cx43 expression at cell borders underscores functional connectivity, essential for COC integrity [4, 29]. In mice, Cx43 loss disrupts granulosa communication and arrests folliculogenesis [30], while electrophysiological studies links its depletion to impaired oocyte competence and follicle development [31]. This robust Cx43 presence likely bolsters the sustained viability and steroidogenesis observed here. In the native COC, communication between cumulus cells and the oocyte is mediated by trans-zonal projections (TZPs), actin-based cytoplasmic extensions that traverse the zona pellucida. As the present model is oocyte-free, true TZPs cannot form. Nevertheless, the strong Cx43 expression observed at cell–cell interfaces indicate preserved gap-junctional coupling among cumulus cells, representing a key component of COC communication.

ECM profiling revealed collagen III, collagen IV, and fibronectin deposition, aligning with gonadotropin-induced COL3A1 upregulation in IVF-derived cumulus

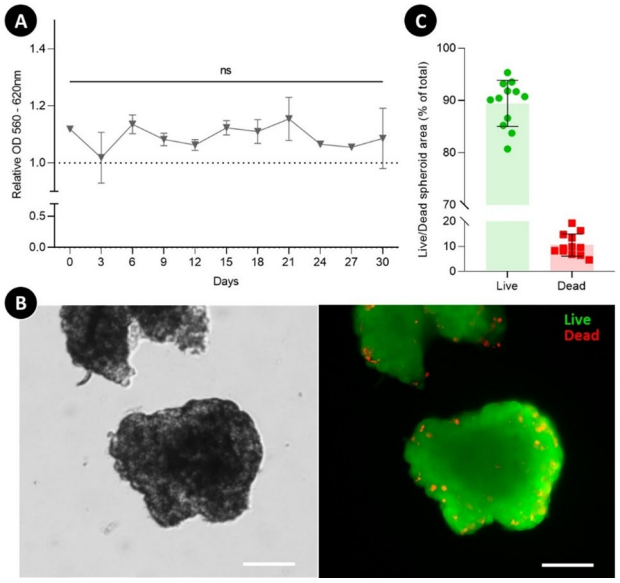

Fig. 5 Metabolic activity and viability of hCGCs spheroids in PEGylated fibrin. **A** Relative absorbance (560–620 nm) via PrestoBlue assay. Experiments were performed with 3 independent biological replicates ($n = 3$) per time point, each consisting of one PEGylated fibrin construct containing three hCGC spheroids derived from pooled of hCGCs obtained from 4–6 patients. Data are presented as mean ± SEM (one-way ANOVA with Geisser-Greenhouse) and normalized to the control of PEGylated fibrin without spheroids (dotted line, Y = 1). **B** Day-30 images: brightfield (left) and Live/Dead staining (right; green = Calcein-AM, red = Ethidium homodimer-1). Scale bars = 100 µm. **C** Viability quantification from Live/Dead staining ($n = 4$ biological replicates; 3 spheroids per replicate). All individual spheroids values are presented; measurements were averaged per biological replicate. Data is presented as mean ± SEM

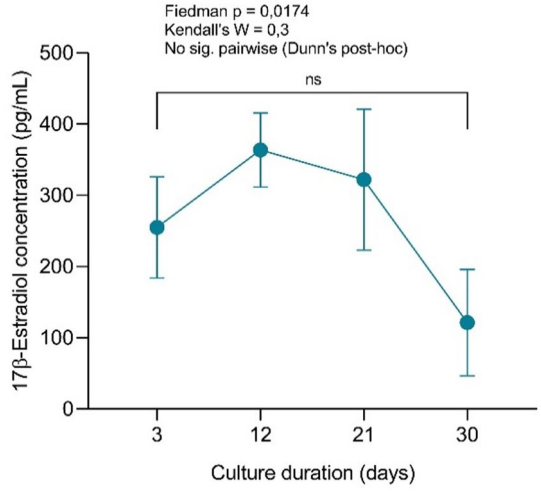

Fig. 6 17β-Estradiol secretion by hCGC spheroids over 30 days. Data represent mean ± SEM from 3 independent biological replicates per time point ($n = 3$), each consisting of three hCGC spheroids derived from pooled cells. Hormone levels were measured in technical duplicated and averaged per biological replicate. Asterisk indicates a significant overall effect of time by Friedman test ($p = 0.0174$, Kendall's W = 0.30, moderate effect size). No significant pairwise differences (Dunn's test, $p > 0.0685$)

cells [32]. These components, though limited in native CGCs [33], may stabilize spheroid architecture via culture-induced adaptation, potentially driven by Menopur's FSH activity. Supporting evidence from rodent and bovine models shows FSH stimulates collagen IV expression [34, 35], a pathway meriting validation in hCGCs. Laminin, a hallmark of MGC basal lamina, was absent, reinforcing the model's cumulus specificity [36]. This ECM profile, free of MGC contamination, enhances fidelity for cumulus-oocyte studies and could inform personalized IVM protocols, as proteomic confirmation might reveal subtype-specific adaptations.

HA is a cornerstone of the cumulus matrix [37], maintaining structure and driving follicle expansion and ovulation in mice [38]. In our model, HA was restored by day 6 despite initial hyaluronidase exposure, which may reflect HA re-synthesis under the culture conditions, consistent with previous reports of gonadotropin-regulated HA production [37, 39]. However, observations could reflect prior exposure of the cells to ovarian stimulation (FSH plus hCG triggering in vivo) and/or continued FSH exposure in vitro, rather than a specific effect of FSH alone. Additional studies are needed to clarify the respective roles of prior in vivo stimulation and in vitro FSH exposure.

Cumulus expansion is a peri-ovulatory process driven by LH/hCG and characterized by HA-rich matrix deposition. Although HA production suggests preservation of key expansion components, functional expansion in response to ovulatory stimuli was not assessed. Future studies should evaluate responsiveness to hCG. Fibronectin's adhesive properties [40] complement HA, enabling ECM reconstruction that mimics native cumulus and bolsters spheroid stability for IVM applications.

Encapsulation in PEGylated fibrin provided ovarian-like mechanics and degradation resistance [41], hypothesizing structural and biochemical support for long-term function. Morphological dynamics, i.e., area and solidity increase by day 15 ($p < 0.01$), stabilizing thereafter at levels comparable to day 0, indicate initial remodeling to a steady state, with the 30-day endpoint. Preliminary observations from our laboratory indicate that primary human cumulus cells exhibit low proliferative activity in vitro. Therefore, the observed increase in spheroid solidity likely reflect structural compaction, ECM remodeling, or HA-mediated expansion rather than an increase in cell number.

Metabolic stability and high viability contrast sharply with 2D degeneration [15], affirming PEGylated fibrin's supportive niche. While recent 3D granulosa models, such as silk-based Silk-Ovaroids or Wharton's jelly/alginate composites [42–44], highlight hydrogel versatility, our CGC-focused system's 30-day steroidogenic

maintenance offers a targeted advantage for oocyte-independent, somatic-only platforms.

Spheroids exhibited dynamic steroidogenesis: estradiol peaked at 370 ± 45 pg/mL (day 12) before declining ~ 50% by day 30 (Friedman test, $p = 0.0174$; Kendall's W = 0.30), uncoupled from viability loss (only 10.6 ± 4.4% dead area). This may reflect gonadotropin-induced transcript switching or FSH receptor adaptation, as observed in mural/cumulus differentiation models where sustained FSH downregulates CYP19A1 and FSHR via internalization [42, 43]. Such dynamics mirror peri-ovulatory shifts, providing a tunable endocrine readout for mechanistic studies.

As described in follicle encapsulation studies, follicular expasion and steroidogenic activity are highly dependent on the physical properties of the surrounding matrix. Following encapsulation, cells undergo an initial adaptation phase and subsequently contribute to matrix production and remodeling, thereby altering the local mechanical environment over time [44, 45]. In our system, spheroid area consistently increased until day 15 and subsequently declined toward values comparable to baseline, paralleling the transient peak in estradiol production. Such dynamics are consistent with progressive remodeling of the PEGylated fibrin matrix, and potentially hydrogel swelling, which together may alter the mechanical and diffusive properties of the microenvironment over time. Some studies showed that in stiffer matrices, follicle expansion is typically constrained, and size may initially increase but subsequently stabilize or decline rather than continuing to enlarge [44, 45]. These temporal changes likely reflect dynamic cell–matrix interactions as the system evolves toward mechanical homeostasis within the encapsulated microenvironment. Importantly, the reduction in area and estradiol production was not accompanied by a marked loss of viability, suggesting functional adaptation rather than progressive cellular degeneration.

Several factors temper generalizability. Limited biological replicates and patient heterogeneity drove variability in estradiol, though post-hoc power analysis confirms exploratory insights. Analysis during the encapsulation period were not feasible due to limited availability of primary cumulus cells. Estradiol decline may also reflect reduced CYP19A1 and/or FSHR expression or diminished availability of upstream androgen subtracts, warranting further validation. In addition, the persistence of endocrine responsiveness relative to basal conditions cannot be directly determined. Future studies incorporating withdrawal or re-stimulation paradigms will be required to evaluate long-term gonadotropin sensitivity more precisely. Oocyte co-culture absence limits COC synergy evaluation. Larger cohorts, RNA-seq for transcriptomic shifts, and denuded oocyte integration could refine the model, extending utility via organoid hybrids for personalized toxicology or OTO-IVM.

Importantly, cumulus cells used in this study were derived from oocytes at different maturation stages, including germinal vesicle (GV), metaphase I (MI), and metaphase II (MII). Cells retrieved from different stages of oocyte maturation could respond differently to this protocol. By pooling cells from multiple developmental stages, this study reflects the diversity encountered in clinical ART practice, although stage-specific responses cannot be distinguished. Future studies using stage-defined cumulus populations will be required to delineate maturation-stage–specific effects, particularly in conditions characterized by a higher proportion of immature oocytes, such as PCOS.

Overall, this platform enables CGC functional adaptation studies and prolonged-exposure assays, such as reproductive toxicology assays or pharmacological testing. In fertility preservation, it aligns with current international guidelines and emerging clinical strategies for ovarian reconstruction in premature ovarian insufficiency, facilitating personalized screening in ART/PCOS patients or somatic optimization in oncology-related OTO-IVM. While intact COCs remain the gold standard for modeling direct oocyte-somatic interactions, our oocyte-independent system provides a complementary tool for isolating and studying granulosa-specific mechanisms in a controlled 3D environment.

Acknowledgements
We thank the IVF Department of UCLouvain's Saint-Luc Hospital for donating granulosa cells for this study. We also wish to express our sincere appreciation to Dr. Arthur Colson (Cliniques universitaires Saint-Luc, UCLouvain) for providing the human placenta and umbilical cord slides used for staining.

Authors' contributions
M.J.S.: conceptualization, methodology, validation, formal analysis, investigation and writing; K.W.: methodology and writing; T.F.R.R.: conceptualization, methodology and validation; M.C.C.: methodology; A.D.: writing, methodology; H.V.: conceptualization and investigation; C.W.: sample administration and review; H.V.: review and supervision; C.A.A.: conceptualization, resources, writing, review, supervision, project administration, and funding acquisition.

Funding
This study was supported by grants from the Fonds National de la Recherche Scientifique (FNRS-PDR Convention grant number T.0004.20 awarded to C.A.A., Ph.D. scholarship awarded to H.V., grant 7.4505.25 F awarded to C.A.A., scholarship awarded to T.F.R.R., and grant FC 51543 awarded to A.D.), and the UCLouvain's Fonds spéciaux de recherche (IREC FSR22, awarded to C.A.A., Ph.D. scholarship awarded to M.J.S.).

Data availability
The data that support the findings of this study are available from the corresponding author, Christiani A. Amorim, upon reasonable request.

Declarations

Competing interests
The authors declare no competing interests.

Author details
[1]Pôle de Recherche en Physiopathologie de la Reproduction, Institut de Recherche Expérimentale et Clinique, Université Catholique de Louvain, Brussels, Belgium
[2]Department of Structural and Functional Biology, Institute of Biology, State University of Campinas, Campinas, São Paulo, Brazil
[3]Department of Gynecology and Andrology, Cliniques Universitaires Saint- Luc, Brussels, Belgium
[4]Laboratory of Tissue Plasticity in Health and Disease, Cluster of Stem Cell and Developmental Biology, Department of Development and Regeneration, KU Leuven, Leuven, Belgium

Received: 2 December 2025 / Accepted: 13 March 2026
Published online: 19 March 2026

References

1. Eppig JJ. Oocyte control of ovarian follicular development and function in mammals. Reproduction. 2001;122(6):829–38.
2. Richards JS, Pangas SA. The ovary: basic biology and clinical implications. J Clin Invest. 2010;120(4):963–72.
3. Garcia-Alonso L, et al. Single-cell roadmap of human gonadal development. Nature. 2022;607(7919):540–7.
4. Xie J, Xu X, Liu S. Intercellular communication in the cumulus–oocyte complex during folliculogenesis: A review. Front Cell Dev Biology. 2023;11:1087612.
5. Clarke HJ. Transzonal projections: Essential structures mediating intercellular communication in the mammalian ovarian follicle. Mol Reprod Dev. 2022;89(11):509–25.
6. Salustri A, et al. Localization and synthesis of hyaluronic acid in the cumulus cells and mural granulosa cells of the preovulatory follicle. Dev Biol. 1992;151(2):541–51.
7. Feuerstein P, et al. Gene expression in human cumulus cells: one approach to oocyte competence. Hum Reprod. 2007;22(12):3069–77.
8. Gilchrist RB, Smitz J. Oocyte in vitro maturation: physiological basis and application to clinical practice. Fertil Steril. 2023;119(4):524–39.
9. Brouillet S et al. Cryopreservation of Oocytes retrieved from Ovarian tissue to optimize fertility preservation in Prepubertal girls and women. J Vis Exp. 2020;(164);e16777. https://doi.org/10.3791/61777.
10. Bourg M, et al. Is in vitro maturation of oocytes retrieved ex vivo from ovarian tissue an effective fertility preservation technique in the presence of organic ovarian cysts? Eur J Obstet Gynecol Reprod Biol. 2023;281:87–91.
11. Gilchrist RB, Lane M, Thompson JG. Oocyte-secreted factors: regulators of cumulus cell function and oocyte quality. Hum Reprod Update. 2008;14(2):159–77.
12. Virant-Klun I, et al. Human oocyte maturation in vitro is improved by co-culture with cumulus cells from mature oocytes. Reprod Biomed Online. 2018;36(5):508–23.
13. Walls ML, et al. In vitro maturation as an alternative to standard in vitro fertilization for patients diagnosed with polycystic ovaries: a comparative analysis of fresh, frozen and cumulative cycle outcomes. Hum Reprod. 2015;30(1):88–96.
14. Hughes SF, Haney AF, Hughes CL Jr. Use of human cumulus granulosa cells for in vitro screening of reproductive toxicants. Reprod Toxicol. 1990;4(1):11–5.
15. Chermuła B, et al. Human cumulus cells in long-term in vitro culture reflect differential expression profile of genes responsible for planned cell death and aging—a study of new molecular markers. Cells. 2020;9(5):1265.
16. Ferronato GA, Vit FF. da Silveira, 3D culture applied to reproduction in females: possibilities and perspectives. Anim Reprod. 2024;21(1):e20230039.
17. Dadashzadeh A, et al. Engineering the ovarian niche: Environmental control of folliculogenesis in vitro. Semin Cell Dev Biol. 2025;175:103639.
18. Sousa MJ, Amorim CA. Engineering cell-based ovarian hormone therapy. Nat Reviews Bioeng. 2025;3(8):620–2.
19. Hummitzsch K, et al. Spheroids of granulosa cells provide an in vitro model for programmed cell death coupled to steroidogenesis. Differentiation. 2009;77(1):60–9.
20. Hryciuk MM, et al. Spheroid formation and luteinization of granulosa cells of felids in a long-term 3D culture. Differentiation. 2023;131:38–48.
21. Ip BC, et al. 3D Microtissues Mimic the Architecture, Estradiol Synthesis, and Gap Junction Intercellular Communication of the Avascular Granulosa. Toxicol Sci. 2022;186(1):29–42.
22. Krotz SP, et al. In vitro maturation of oocytes via the pre-fabricated self-assembled artificial human ovary. J Assist Reprod Genet. 2010;27(12):743–50.
23. Chiti MC, Amorim CA, Dolmans M-M. Fibrin-based artificial ovary prototype: from animal models to human clinical application. Curr Trends Clin Embryol. 2018;5(3):122–9.
24. Almany L, Seliktar D. Biosynthetic hydrogel scaffolds made from fibrinogen and polyethylene glycol for 3D cell cultures. Biomaterials. 2005;26(15):2467–77.
25. Vanderslice EJ, Golding SGH, Jacot JG. Vascularization of PEGylated fibrin hydrogels increases the proliferation of human iPSC-cardiomyocytes. J Biomed Mater Res A. 2024;112(4):625–34.
26. Dadashzadeh A, Moghassemi S, Amorim CA. Evaluation of PEGylated fibrin as a three-dimensional biodegradable scaffold for ovarian tissue engineering. Mater Today Chem. 2021;22:100626.
27. Dadashzadeh A, et al. Mind the mechanical strength: tailoring a 3D matrix to encapsulate isolated human preantral follicles. Hum Reprod open. 2023;2023(2):hoad004.
28. Tahajjodi SS, et al. Biological and physiological characteristics of human cumulus cells in adherent culture condition. Int J reproductive Biomed. 2020;18(1):1.
29. Kidder GM, Mhawi AA. Gap junctions and ovarian folliculogenesis. REPRODUCTION-CAMBRIDGE-. 2002;123(5):613–20.
30. Ackert CL, et al. Intercellular communication via connexin43 gap junctions is required for ovarian folliculogenesis in the mouse. Dev Biol. 2001;233(2):258–70.
31. Tong D, et al. Patch-clamp study reveals that the importance of connexin43-mediated gap junctional communication for ovarian folliculogenesis is strain specific in the mouse. Am J Physiology-Cell Physiol. 2006;290(1):C290–7.
32. Assou S, et al. Comparative gene expression profiling in human cumulus cells according to ovarian gonadotropin treatments. Biomed Res Int. 2013;2013(1):354582.
33. Lind A-K, et al. Collagens in the human ovary and their changes in the perifollicular stroma during ovulation. Acta Obstet Gynecol Scand. 2006;85(12):1476–84.
34. Adriaenssens T, et al. Differences in collagen expression in cumulus cells after exposure to highly purified menotropin or recombinant follicle-stimulating hormone in a mouse follicle culture model. Biol Reprod. 2009;80(5):1015–25.
35. Šutovský P, Fléchon JE, Pavlok A. F-actin is involved in control of bovine cumulus expansion. Mol Reprod Dev. 1995;41(4):521–9.
36. Familiari G, et al. Heterogenous distribution of fibronectin, tenascin-c, and laminin immunoreactive material in the cumulus-coronal cells surrounding mature human oocytes from IVF-ET protocols—Evidence that they are composed of different subpopulations: An immunohistochemical study using scanning confocal laser and fluorescence microscopy. Mol Reprod Development: Incorporating Gamete Res. 1996;43(3):392–402.
37. Nagyova E. The biological role of hyaluronan-rich oocyte-cumulus extracellular matrix in female reproduction. Int J Mol Sci. 2018;19(1):283.
38. Thomas C, et al. Ex vivo imaging reveals the spatiotemporal control of ovulation. Nat Cell Biol. 2024;26(11):1997–2008.
39. Kimura N, et al. Expression of hyaluronan synthases and CD44 messenger RNAs in porcine cumulus-oocyte complexes during in vitro maturation. Biol Reprod. 2002;66(3):707–17.
40. Kitasaka H, et al. Inductions of granulosa cell luteinization and cumulus expansion are dependent on the fibronectin-integrin pathway during ovulation process in mice. PLoS ONE. 2018;13(2):e0192458.
41. Ouni E, et al. A blueprint of the topology and mechanics of the human ovary for next-generation bioengineering and diagnosis. Nat Commun. 2021;12(1):5603.
42. Casarini L, Crépieux P. Molecular mechanisms of action of FSH. Front Endocrinol. 2019;10:305.
43. Sanford JC, Batten BE. Endocytosis of follicle-stimulating hormone by ovarian granulosa cells: Analysis of hormone processing and receptor dynamics. J Cell Physiol. 1989;138(1):154–64.
44. West ER, et al. Physical properties of alginate hydrogels and their effects on in vitro follicle development. Biomaterials. 2007;28(30):4439–48.

45. Pietroforte S, Amargant F. Increased stiffness mimicking ovarian aging induces a fibroinflammatory response in follicles and impairs oocyte quality. Reproduction. 2026;171(2):xaaf026. https://doi.org/10.1093/reprod/xaaf026.

Publisher's note